ChemSusChem
doi.org/10.1002/cssc.202001717



# Reverse Semi-Combustion Driven by Titanium Dioxide-Ionic Liquid Hybrid Photocatalyst

Muhammad I. Qadir,[a, b] Marcileia Zanatta,[a, c] Jose Pinto,[d] Isabel Vicente,[e] Aitor Gual,[e] Emily F. Smith,[d] Brenno A. D. Neto,[f] Paulo E. N. de Souza,[g] Sherdil Khan,[h] Jairton Dupont,*[a] and Jesum Alves Fernandes*[d]

Unprecedented metal-free photocatalytic $CO_2$ conversion to CO (up to $228 \pm 48\ \mu mol\ g^{-1}\ h^{-1}$) was displayed by $TiO_2$@IL hybrid photocatalysts prepared by simple impregnation of commercially available P25-titanium dioxide with imidazolium-based ionic liquids (ILs). The high activity of $TiO_2$@IL hybrid photocatalysts was mainly associated to (i) $TiO_2$@IL red shift compared to the pure $TiO_2$ absorption, and thus a modification of the $TiO_2$ surface electronic structure; (ii) $TiO_2$ with IL bearing imidazolate anions lowered the $CO_2$ activation energy barrier. The reaction mechanism was postulated to occur via $CO_2$ photoreduction to formate species by the imidazole/imidazole radical redox pair, yielding CO and water.

## Introduction

During the last decade, many research efforts have been focussed on the development of efficient catalytic processes involving the use of renewable energy sources for the carbon neutral transformation of carbon dioxide ($CO_2$) to fuels and chemicals.[1] Among them, $CO_2$ photoreduction to intermediates for chemical synthesis [carbon monoxide (CO)] and/or solar fuels for storage/transport of energy in the form of hydrocarbons (artificial photosynthesis) has grown into a blooming field of research.[2] A simple combination of sunlight, aqueous solutions saturated with $CO_2$ and an appropriate photocatalysts may yield CO (reverse semi-combustion) and/or solar fuel hydrocarbons (reverse combustion).[3] However, the high energy barrier of $CO_2$ activation, side reactions (such as hydrogen evolution) and high rates of electron-hole pair recombination of the photocatalysts employed still remain as unsolved challenges.[4] Although great advances have been made to enhance the $CO_2$ photoreduction, the photocatalytic performance (in terms of activity and/or selectivity) reported so far still remain low compared to conventional $CO_2$ reduction processes (i.e., $CO_2$ thermal reduction and $CO_2$ electroreduction).[2b] Most of the current $CO_2$ photoreduction approaches encompass only one side of the reaction by (i) designing new photocatalysts to extend the visible absorption and supress the electron-hole recombination (ii) or aiming to overcome the formation of the undesired high-energy intermediate species.[5] Therefore, a fresh approach that embraces both sides of the reaction (semiconductor properties and $CO_2$ activation) should be sought to unlock the next generation of photocatalysts for competitive and efficient $CO_2$ photoreduction by innovative approach exploiting fleeting open-shell intermediates, such as radical ions and radicals.[6]

Titanium dioxide ($TiO_2$) has been widely studied as a photocatalyst in the production of solar fuels,[7] however, still displaying low photocatalytic activity for the $CO_2$ conversion, either, to CO and solar fuel hydrocarbons (Table S2).[8] Among others, the most utilised strategy for the enhancement of the $TiO_2$ photocatalytic performance, involve the structural and surface fine tuning by incorporation of other semiconductors (i.e., Z-schemes),[9] dopants,[10] metal-nanoparticles,[11] thus shifting the absorption edge to the visible light.[3a]

The pH of the reaction media, and thus, the concentration in solution by the formation of carbonate ($[CO_3]^{2-}$) and bicarbonate ($[HCO_3^-]$) species is also an important factor for enhancing the $CO_2$-tranformation reaction rate kinetics. For instance, the superior $CO_2$-transformation performance of $TiO_2$ anatase (001) surface is explained by a stronger basicity of the

[a] Dr. M. I. Qadir, Dr. M. Zanatta, Prof. J. Dupont
Institute of Chemistry, Federal University of Rio Grande do Sul
Campus Agronomia, Porto Alegre, 90650-001 (Brazil)
E-mail: jairton.dupont@ufrgs.br
[b] Dr. M. I. Qadir
Department of Nanocatalysis, J. Heyrovský Institute of Physical Chemistry, Czech Academy of Sciences, Dolejškova 2155/3, 18223 Prague 8, (Czech Republic)
[c] Dr. M. Zanatta
i3N|Cenimat, Department of Materials Science, NOVA School of Science and Technology
NOVA University Lisbon
2829-516 Caparica (Portugal)
[d] J. Pinto, Dr. E. F. Smith, Dr. J. Alves Fernandes
School of Chemistry, University of Nottingham
University Park, Nottingham, NG7 2RD (United Kingdom)
E-mail: jesum.alvesfernandes@nottingham.ac.uk
[e] Dr. I. Vicente, Dr. A. Gual
Unitat de Tecnologíe Químiques, EURECAT
Tarragona, 43007 (Spain)
[f] Prof. B. A. D. Neto
Institute of chemistry, University of Brasília
Campus Universitário Darcy Ribeiro, Brasília, 70904-970 (Brazil)
[g] Prof. P. E. N. de Souza
Institute of Physics, University of Brasília
Campus Universitário Darcy Ribeiro, Brasília, 70904-970 (Brazil)
[h] Dr. S. Khan
Institute of Physics, Federal University of Rio Grande do Sul
Campus Agronomia, Porto Alegre, 90650-001 (Brazil)

Supporting information for this article is available on the WWW under https://doi.org/10.1002/cssc.202001717

surface oxygen sites.[12] Most importantly, mass transfer limitations plays a crucial role, since compared to the gas-solid interface, the energy barrier for the liquid-solid $CO_2$-photocatalysed reduction is reduced by 0.05–0.25 eV in aqueous saturated $CO_2$ solutions with high bicarbonate ($[HCO_3^-]$) concentrations. The water solvation effect can greatly decrease the energy barrier of $CO_2$ reduction and also affect the selectivity of the reaction processes by providing water dissociation species involved in most of the common $CO_2$-reduction equations (i.e., protons ($[H^+]$) or hydroxy species ($[OH^-]$)).[13]

Imidazolium-based ionic liquids (ILs) have been recognized to solubilize and activate $CO_2$ by stabilizing radical/anionic species[14] and hence, may constitute an attractive material for $CO_2$ photoreduction.[15]

Therefore, combining ILs with semiconductors is a promising strategy towards the modification of physical-chemical properties of the semiconductors (Figure 1).[16]

Recently, many studies have been focussing on the interaction of ILs and semiconductors.[17] Based on elegant theoretical calculations, the interactions of ILs with $TiO_2$ have been proposed to affect and modulate the electronic properties of the $TiO_2$ surface (i.e., valence and conduction band edge energies and modification of the band gap).[18] In this case, the IL may provide the driving force towards photocatalytic redox process by formation of a solid semiconductor-liquid junction improving the charge separation and tuning the electron/hole ratio. Moreover, aqueous solution of ILs containing basic anions when in contact with $CO_2$ can favour its solubilisation by bicarbonates ($[HCO_3^-]$) concentrations[19] and decrease the energy barrier of $CO_2$ reduction.[14a,20]

Herein, we demonstrate that the simple impregnation of commercially available P25-$TiO_2$ with imidazolium ILs generates highly efficient hybrid photocatalysts for the $CO_2$ reduction to CO with unprecedented catalytic activity. We demonstrate that the enhancement of the $CO_2$-photocalytic performance is associated to (i) a shift of the $TiO_2$@IL valence and conduction band edge with simultaneously decreasing the band gap when compared to bare $TiO_2$; (ii) continuous generation of formate species via imidazole/imidazole radical redox pair lowered the activation barrier energy of $CO_2$ photoreduction (Figure 1).

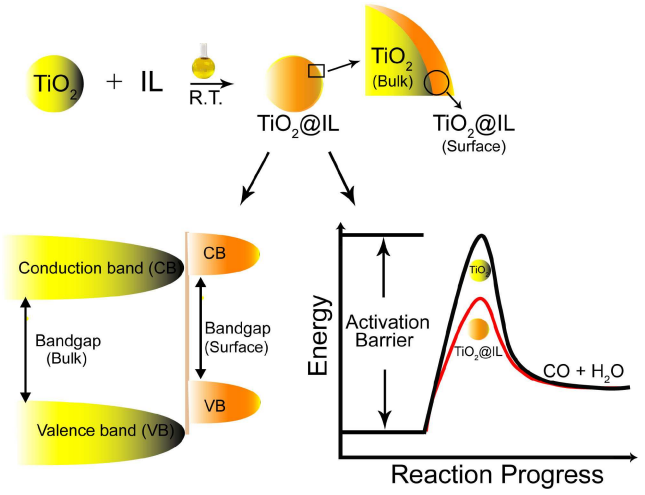


**Figure 1.** Schematic representation of expected effects induced by ILs on $TiO_2$ surface for photoreduction of $CO_2$ in aqueous solution. a) $TiO_2$@IL hybrid photocatalyst preparation. b) $TiO_2$@IL surface valence and conduction band edge shift with simultaneously decreasing the band gap when compared to bare $TiO_2$. c) $TiO_2$@IL lowering the activation barrier energy of $CO_2$ photoreduction, similar to proposed for electroreduction of $CO_2$ to CO by Masel and co-workers.[14a]

## Results and Discussion

The photoreduction of $CO_2$ was first performed in aqueous solution of ILs,[21] without the presence of $TiO_2$ (Table 1). The ILs 1-*n*-butyl-3-methylimidazolium bis(trifluoromethylsulfonyl)imide ($[BMIm][NTf_2]$) and 1-*n*-butyl-3-methylimidazolium chloride ([BMIm]Cl) ILs did not show production of CO (Table 1, entries 1 and 2). In contrast to ILs with $[NTf_2^-]$ and $Cl^-$ anions, ILs with imidazolate anion ([Im]) 1-*n*-butyl-3-methylimidazolium imidazolate ([BMIm][Im]) displayed $CO_2$ photoreduction to CO up to $62 \pm 30\ \mu mol\ g^{-1}$ with selectivity higher than 99% (Table 1, entry 3).

There is a noteworthy influence of the anion on $CO_2$ photoreduction (Table 1, entries 1–5). CO is produced only with ILs containing basic anions (imidazolate), indicating their involvement (direct or indirect) on the $CO_2$ activation, $H_2O$ oxidation, and probably also on the confinement of the photocatalyst active sites in water-deficient media, in which the $CO_2$ reduction mechanism follows distinct reaction pathways than in $H_2O$-rich media (i.e., higher $H_2$ selectivity in $H_2O$-rich media). It is important to note that on replacing the imidazolium cation with pyrrolidinium and phosphonium cation, ILs also produced a significant amount of CO, approximately $60 \pm 32$ and $89 \pm 38\ \mu mol\ g^{-1}$ with [BMPy][Im] and $[(But)_3EP][Im]$ ILs, respectively (Table 1, entries 4 and 5). This can be related to the presence of imidazolate anion not only increasing the sorption of $CO_2$ but also increasing the local basicity. The photoreduction of $^{13}CO_2$ with the aqueous solution of [BMIm][Im] was performed to verify that CO is produced from the $CO_2$ by photoreduction leading to $^{13}CO$ detected at $m/z = 29$ by GC-MS (Figure S11). Of note, no CO was observed when the reactions were performed under dark using ILs.

$TiO_2$@IL hybrid photocatalysts were prepared by simple mixing of P25-$TiO_2$ (AEROXIDE $TiO_2$ P25)[22] with [BMIm][Im], $[BMIm][NTf_2]$, [BMIm]Cl, [BMPy][Im] and $[(But)_3EP][Im]$ ILs at room temperature, in water or chloroform yielding a similar IL

**Table 1.** Summary of photoreduction performance for $CO_2$ reduction using IL in aqueous media.[a]

| Entry | Catalyst | IL [mg] | CO [$\mu mol\ g^{-1}$] |
|---|---|---|---|
| 1 | [BMIm]Cl | 0.8 | – |
| 2 | $[BMIm][NTf_2]$ | 0.8 | – |
| 3 | [BMIm][Im] | 0.8 | $62 \pm 30$ |
| 4 | [BMPy][Im] | 0.8 | $60 \pm 32$ |
| 5 | $[(But)_3EP][Im]$ | 0.8 | $89 \pm 38$ |

Reaction conditions: [a] $CO_2$ (atmospheric pressure), $H_2O$ (2 mL), 25 °C, Xe lamp (300 W), 2 h. CO production values have been obtained from at least three experiments.

loading for all of them (see the Supporting Information for details). Brunauer-Emmett-Teller (BET) analyses show that both the $TiO_2$ surface area and pore volume are significantly reduced after IL impregnation (Table S1 and Figure S5b). These results indicate that the ILs are well distributed among $TiO_2$ grains in addition to uniformly filling the apparent porosity created by interstitial space between $TiO_2$ grains.

It is important to mention that IL (cations and anions) coordination on $TiO_2$ surface is still not fully understood; however, it has been accepted that cations and anions coordinate to different $TiO_2$ sites.[17b,18,23] The $TiO_2$ surface offers either O or Ti atoms for ionic coordination; positively charged cations coordinate to the O atom and negatively charged anions coordinate to Ti atoms.[18] For $TiO_2$, the valence band predominantly consists of O 2p states, and the conduction band is mainly composed of Ti 3d states.[24] Therefore, $TiO_2$ band edge shift depends on the amount of electronic charge accepted/donated from the IL to $TiO_2$ or vice versa.[18] In order to investigate these effects UV/Vis and X-ray photoelectron spectroscopy (XPS) measurements of $TiO_2$@IL hybrid photocatalysts were performed.

UV/Vis measurements of $TiO_2$@IL revealed a red shift ($\approx$0.2 eV) compared with bare $TiO_2$, regardless of the type of IL used (Figure 2a). These results are in agreement with theoretical calculations on $TiO_2$@IL interaction, in which a red shift between 0.1 to 0.4 eV is predicted.[18] XPS wide-scan and high-resolution spectra of C 1 s and Ti 2p from all $TiO_2$@IL can be found in the Supporting Information (Figures S7 and S8). From the valence band XPS analyses (Figure 2b), the valence band maximum (VBM) of bare $TiO_2$ surface was observed at approximately 5 eV ascribed to O 2p–Ti 4sp $\pi$ bonding and the higher binding energy state was observed at approximately 7.5 eV that is assigned to O 2p–Ti 3d $\sigma$ bonding.[24,25] On the other hand, a new structure at $TiO_2$ surface is observed for $TiO_2$@[BMIm][Im] by a shift of the VBM (0.25 eV) towards the Fermi energy $E_f$. The shift of VBM at lower energy in the $TiO_2$ system can be ascribed to the presence of new surface states within the $TiO_2$ and IL interface (a control experiment is displayed in the Figure S9).

The $TiO_2$@[BMIm][Im] upward shift of VBM of 0.25 eV led to an upward shift of the conduction band maximum (CBM) of 0.05 eV. The upward shift of VB and CB suggests a higher amount of charge transfer between IL anion and $TiO_2$ surface compared to IL cation withdrawing charge from $TiO_2$ surface. However, for $TiO_2$@[BMPy][Im] and $TiO_2$@[$(But)_3$EP][Im] a positive shoulder was detected (Figure 2b), which may suggest a downward shift of VBM and thus a higher cation acceptance charge from $TiO_2$ surface compared to IL anion and $TiO_2$ surface charge transfer. In comparison, for non-basic IL anions, $TiO_2$@[BMIm][$NTf_2$] and $TiO_2$@[BMIm]Cl, the VBM position remained as of bare $TiO_2$. Therefore, the decrease of 0.2 eV in the BG, observed in the UV/Vis measurements, suggest a downward shift of 0.2 eV in the CBM for $TiO_2$@[BMIm][$NTf_2$] and $TiO_2$@[BMIm]Cl. This effect can be ascribed to a weak interaction between anion and $TiO_2$, thus leading to a higher charge donation from $TiO_2$ surface to IL cation.[18] These results confirm that in most of the cases, anions have a dominant influence on energy band shift; however, it also demonstrated that the proper choice of both IL cation and anion can adjust the desired semiconductor physical-chemical properties.

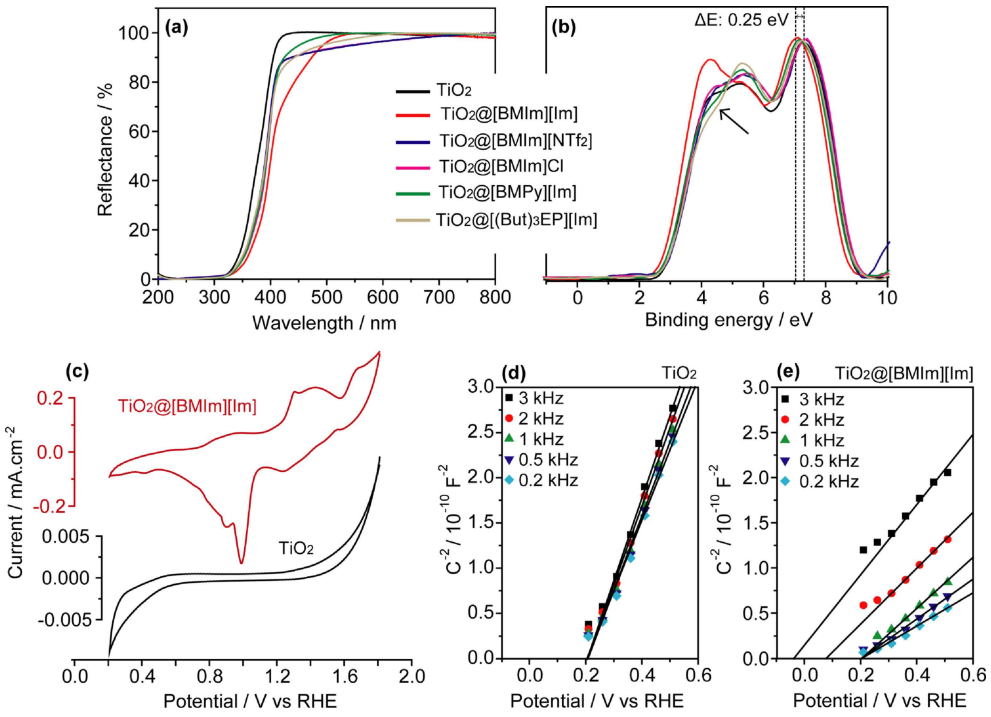


**Figure 2.** (a) Diffuse reflectance spectra and (b) valence band spectra from XPS. Electrochemistry measurements of pure $TiO_2$ versus $TiO_2$@[BMIm][Im]: (c) Cyclic voltammetry and (d, e) Mott-Schottky plots.

To further investigate the effects observed by UV/Vis and XPS, electrochemistry measurements of $TiO_2$ and $TiO_2$@[BMIm][Im] films deposited on fluorine-doped tin oxide (FTO) substrate were performed. A significant difference was recorded in cyclic voltammetry of $TiO_2$@[BMIm][Im] as compared to bare $TiO_2$ (Figures S2c and S10). In line with the literature, bare $TiO_2$ did not exhibit peaks in the voltammograms whereas $TiO_2$@[BMIm][Im] presented distinct redox peaks and an enhancement in current density.[26] The appearance of these peaks suggests generation of oxygen vacancies leading to interband states induced by the IL in $TiO_2$ crystal structure, thereby resulting in higher conductivity of $TiO_2$@[BMIm][Im].[27] This effect has been previously observed, which was associated to the interfacial electric field effect and/or to the water contaminants in ILs.[28] The flat band positions of bare $TiO_2$ and $TiO_2$@[BMIm][Im] were studied through Mott-Schottky (MS) plots (Figure 2d,e). MS plots display positive slopes corresponding to the n-type nature of the samples, however, the slope for $TiO_2$@[BMI][Im] is smaller than the bare $TiO_2$ indicating increased donor densities corroborating to the appearance of redox peaks in cyclic voltammograms (Figure 2c).[29] For bare $TiO_2$ the MS curves converge to approximately 0.2 V vs. reversible hydrogen electrode (RHE) at all applied frequencies. However, $TiO_2$@[BMIm][Im] displays frequency dispersion where at lower frequencies the MS curves converge to approximately 0.2 V vs. RHE and for higher frequencies a negative shift is observed. The validity of MS analyses is based on the fact that series capacitances corresponding to the semiconductor-liquid interfaces are much higher than the capacitance of space charge layer. In case of thin space charge layer (higher defect densities in electrode material), the capacitance such as Helmholtz capacitance may not be neglected, which may result in frequency dispersion.[30] It should be noted that the dispersion in MS plots is a topic of discussion; however, possible reasons to this dispersion are defective nature of the film, interband states, inhomogeneous doping and atomic roughness.[30,31] Therefore, electrochemical, XPS and UV/Vis analyses clearly demonstrated a shift of valence band position and generation of interband states in $TiO_2$ surface due to impregnation of [BMIm][Im] IL.[32]

The photocatalytic experiments of the thus prepared $TiO_2$@IL hybrid photocatalysts were also performed using only water. The obtained results are summarized in Table 2.

Naked $TiO_2$ revealed very low catalytic activity and produced only CO (Table 2, entry 7, $3 \pm 1$ μmol $g^{-1}$). Remarkably, $TiO_2$@[BMIm][Im] hybrid photocatalyst displays generation of CO of $228 \pm 48$ μmol $g^{-1}$ $h^{-1}$ with a selectivity of the 99%, and enhancement of approximately 150 times compared to bare $TiO_2$ and 8 times of that of the bare IL (Table 2, entry 1 and Table 1, entry 3). Moreover, $TiO_2$@[BMIm][Im] displayed an apparent quantum efficiency of 10.9% (using 360 nm band pass filter) as well as showed high stability after recyclability tests performed for three cycles of 12 h each (Figure S14). These are impressive results compared to previous systems using sacrificial agents and noble metals reported to date (Tables S2 and S3). $TiO_2$@[BMIm][Im] catalyst showed the highest activity to CO, as compared to photocatalysts containing the imidazolate anion associate with phosphonium or pyrrolidinium cations (Table 2, entries 2 and 3). These results can be ascribed to higher charge transfer between IL anion and $TiO_2$, and thus the VBM shift of $TiO_2$@[BMIm][Im] compared to $TiO_2$@[BMPy][Im] and $TiO_2$@[$(But)_3$EP][Im]. The $TiO_2$@[BMIm][Im] also displayed higher conversion of $CO_2$ to CO when compared to $TiO_2$@[BMIm]Cl and $TiO_2$@[BMIm][$NTf_2$] (Table 2, entries 4 and 5). In this case, it can be related to a weak interaction between those anions (Cl and [$NTf_2$] anions) and $TiO_2$ surface, and mainly due to the non-basic of Cl and [$NTf_2$] anions.

**Table 2.** Summary of photoreduction performance for $CO_2$ reduction using $TiO_2$@IL hybrid photocatalyst in aqueous media.[a]

| Entry | Catalyst | $TiO_2$@IL [mg] | CO [μmol $g^{-1}$] |
|---|---|---|---|
| 1 | $TiO_2$@[BMIm][Im] | 20[b] | $455 \pm 96$ |
| 2 | $TiO_2$@[BMPy][Im] | 20[b] | $80 \pm 7$ |
| 3 | $TiO_2$@[$(But)_3$EP][Im] | 20[b] | $207 \pm 16$ |
| 4 | $TiO_2$@[BMIm]Cl | 20[b] | $220 \pm 23$ |
| 5 | $TiO_2$@[BMIm][$NTf_2$] | 20[b] | $101 \pm 55$ |
| 6 | $TiO_2$ + [BMIm][Im] | 20[b,c] | $177 \pm 84$ |
| 7 | $TiO_2$ | – | $3 \pm 1$ |

Reaction conditions: [a] $CO_2$ (atmospheric pressure), $H_2O$ (2 mL), 25 °C, Xe lamp (300 W), 2 h. CO production values have been obtained from at least three experiments. [b] The amount of IL used for $TiO_2$@IL can be found in Table S1. [c] A small amount of oxygen was detected along with other major by-products formic acid and bicarbonate (Figures S2–S4).

The $CO_2$ reduction step, the base comes from the activation of water by the imidazolate anion to form an imidazole and [$HCO_3^-$] observed by $^{13}C$ NMR spectroscopy (Figure S3).[19,33] The formation of imidazole radical (Figure S12) can be afford via $TiO_2$ charge transfer, which seems to be very efficient in the $TiO_2$@IL heterojunction-like effect, and $H^+$ abstraction from the water oxidation. The imidazole radical transfer its charge to $CO_2$, then the imidazole is regenerated, and $CO_2$ abstracts a proton and electron to generate formate species, as detected in the liquid phase by $^1H$ and $^{13}C$ NMR spectroscopy (Figures S4 and S3, respectively).[20,34] The formate species generates CO and water, which was confirmed via photocatalytic reaction using aqueous solution of formic acid (without the presence of $CO_2$), which preferentially yielded CO (Figure S13).

## Conclusion

The simple impregnation of $TiO_2$ with imidazolium-based ionic liquid (IL) associated with basic anions generated a new hybrid highly active photocatalyst for the $CO_2$ reduction in water. The observed photocatalytic activity can be related to synergetic effect between ILs and $TiO_2$ that follows the order $TiO_2$@[BMIm][Im] ≫ $TiO_2$@[BMIm]Cl > $TiO_2$@[$(But)_3$EP][Im] ≫ $TiO_2$@[BMIm][$NTf_2$] > $TiO_2$@[BMPy][Im]. The IL plays a dual role by inducing a shift of the valence and conduction band edge energies with simultaneously decreasing the band gap; as well as continuous generation of formate radicals ([$HCO_2^{\bullet}$]) which suggest a decrease of $CO_2$ activation energy barrier and thus improves the catalyst performance (i.e., yield and selectivity to CO). The $CO_2$ reduction reaction proceeds probably via $CO_2$ reaction with

imidazole/imidazole radical redox pair, and then it produces formate species yielding CO and water. This promising approach can be extended to a vast range of photoactive materials (e.g., g-$C_3N_4$) opening a new avenue towards $CO_2$ photoreduction and many others photocatalytic systems.

## Experimental Section

**General**: P25-$TiO_2$ (AEROXIDE $TiO_2$ P25) was purchased from EVINIK and it was used without any previous treatment. The ILs 1-*n*-butyl-3-methylimidazolium imidazolate ([BMIm][Im]), 1-*n*-butyl-1-methylpyrrolidinium imidazolate ([BMPy][Im]) and tri-*n*-butyl-ethyl-phosphonium imidazolate ($[(But)_3EP][Im]$) 1-*n*-butyl-3-methylimidazolium bis(trifluoromethylsulfonyl)imide ($[BMIm][NTf_2]$) and 1-*n*-butyl-3-methylimidazolium chloride ([BMIm]Cl) were prepared according to literature procedures.[35] All the ILs were dried under vacuum and argon for 2 days prior to use. ESR analyses were achieved in a Bruker spectrometer (Bruker EMXplus, Germany), equipped with an X-band (9 GHz) high sensitivity cavity (Bruker ER 4119HS, Germany) using frozen samples inside a quartz finger Dewar filled with liquid nitrogen. 400 μL of the aqueous IL solution (0.22 M for each IL) were collected and transferred to a 1 mL decapped syringe and frozen in liquid nitrogen. The frozen cylindrical samples were transferred to a quartz finger Dewar (Noxygen, Germany) filled with liquid nitrogen, placed inside the resonator and their electron spin resonance (ESR) spectra were recorded at −196 °C. This procedure ensured identical volumes for all samples, allowing the quantitative comparison among the recorded ESR spectra. The instrumental settings were 2 mW microwave power, 10 G amplitude modulation, 100 kHz modulation frequency, 1000 G sweep width, 3365 G central field and 50s sweep time. The peak-to-peak amplitude, that is the difference between the lowest and the highest amplitudes in the first derivative spectrum, was used to detect signal quantification. NMR analyses were performed on a Bruker Avance 400 spectrometer. XPS measurements were performed using a Kratos AXIS Ultra DLD instrument (details can be found in the Supporting Information, section 6). All the electrochemistry measurements were performed using $TiO_2$ and $TiO_2$@[BMIm][Im] films deposited on FTO substrate, with each sample being prepared and measured three times to ensure the reproducibility of the measurements (details can be found in the Supporting Information, section 7). The generated gases during the photocatalytic reaction were quantified by GC using an Agilent 6820 equipped with a Porapak Q 80–100 Mesh column and argon as carrier gas. The gaseous products were simultaneously analysed with a thermal conductivity detector (TCD) and a flame ionization detector (FID). Aliquots of 100 μL from the gas phase were removed from the head of the photoreactor reactor and injected with a syringe containing a Hamilton sample lock valve. After the photocatalysis, the liquid phase was analysed by NMR spectroscopy. For the evolutions of intermediates by NMR analyses all the reactions were performed with 120 mg of IL under our standard conditions. In order to detect the generated $^{13}CO$, a MS (QIC 20®-Hiden Analytical) configured with the ionization of 70 eV was used.

**$CO_2$ photoreduction experiments**: Typically, a Schlenk tube containing 30 mL of degassed milli-Q water was saturated with $CO_2$ (50 bar) at a rate of 2 mL $min^{-1}$ at room temperature. The photocatalysis was performed in a homemade quartz reactor equipped with a water-circulating jacket to maintain the temperature at 25 °C. 2 mL of $CO_2$-saturated water was added in photoreactor containing the desired amount of freshly prepared catalyst under argon atmosphere. After that, $CO_2$ was introduced into the reactor by a filled balloon and stirred at room temperature for 30 min. After removing the $CO_2$ balloon, the reactor was placed in front of 300 W Xe lamp. After desired time, gaseous products were withdrawn by gas-tight syringe from the reactor's headspace and analysed by GC.

## Acknowledgements

*J.A.F. thanks Beacon of excellence: Propulsion Futures and Green Chemicals of the University of Nottingham, to EPSRC CDT in Sustainable Chemistry (EP/L015633/1), and EPSRC: LiPPS XPS system, and EP/K005138/1 "University of Nottingham Equipment Account" for providing financial support for this work. We also thanks to CAPES (158804/2017-01 and 001), FAPERGS (16/2552-0000 18/2551-0000561-4, 88887.195052/2018-00), CNPq (406260/2018-4, 169462/2017-0, 406750/2016-5 and 465454/2014-3) and INCT-Catalise. M.I.Q. also acknowledges support from the European Union's Horizon 2020 research and innovation program under grant agreement No 810310, which corresponds to the J. Heyrovsky Chair project ("ERA Chair at J. Heyrovský Institute of Physical Chemistry AS CR – The institutional approach towards ERA") during the finalization of the paper, which had no role in the preparation of this article. S.K. gratefully acknowledges CAPES-PRINT scientific missions funding to support his visit to UoN.*

## Conflict of Interest

The authors declare no conflict of interest.

**Keywords:** carbon dioxide · carbon monoxide · ionic liquids · photocatalysis · titania

[1] a) J. Artz, T. E. Müller, K. Thenert, J. Kleinekorte, R. Meys, A. Sternberg, A. Bardow, W. Leitner, *Chem. Rev.* **2018**, *118*, 434–504; b) J. Klankermayer, S. Wesselbaum, K. Beydoun, W. Leitner, *Angew. Chem. Int. Ed.* **2016**, *55*, 7296–7343; *Angew. Chem.* **2016**, *128*, 7416–7467; c) D. Faggion, W. D. G. Gonçalves, J. Dupont, *Front. Chem.* **2019**, *7*, 102?.
[2] a) T. A. Faunce, W. Lubitz, A. W. Rutherford, D. MacFarlane, G. F. Moore, P. Yang, D. G. Nocera, T. A. Moore, D. H. Gregory, S. Fukuzumi, K. B. Yoon, F. A. Armstrong, M. R. Wasielewski, S. Styring, *Energy Environ. Sci.* **2013**, *6*, 695–698; b) K. Li, B. Peng, T. Peng, *ACS Catal.* **2016**, *6*, 7485–7527.
[3] a) J. L. White, M. F. Baruch, J. E. Pander, Y. Hu, I. C. Fortmeyer, J. E. Park, T. Zhang, K. Liao, J. Gu, Y. Yan, T. W. Shaw, E. Abelev, A. B. Bocarsly, *Chem. Rev.* **2015**, *115*, 12888–12935; b) S. N. Habisreutinger, L. Schmidt-Mende, J. K. Stolarczyk, *Angew. Chem. Int. Ed.* **2013**, *52*, 7372–7408; *Angew. Chem.* **2013**, *125*, 7516–7557.
[4] a) S. Wang, B. Y. Guan, X. W. Lou, *Energy Environ. Sci.* **2018**, *11*, 306–310; b) J. Ran, M. Jaroniec, S.-Z. Qiao, *Adv. Mater.* **2018**, *30*, 1704649–n/a.
[5] K. Teramura, K. Hori, Y. Terao, Z. Huang, S. Iguchi, Z. Wang, H. Asakura, S. Hosokawa, T. Tanaka, *J. Phys. Chem. C* **2017**, *121*, 8711–8721.
[6] L. Capaldo, L. L. Quadri, D. Ravelli, *Angew. Chem. Int. Ed.* **2019**, *58*, 17508–17510; *Angew. Chem.* **2019**, *131*, 17670–17672.
[7] Y. Liao, S.-W. Cao, Y. Yuan, Q. Gu, Z. Zhang, C. Xue, *Chem. Eur. J.* **2014**, *20*, 10220–10222.
[8] a) S. Xie, Y. Wang, Q. Zhang, W. Deng, Y. Wang, *ACS Catal.* **2014**, *4*, 3644–3653; b) S. Kumar, L. J. Durndell, J. C. Manayil, M. A. Isaacs, C. M. A. Parlett, S. Karthikeyan, R. E. Douthwaite, B. Coulson, K. Wilson, A. F. Lee, *Part. Part. Syst. Charact.* **2018**, *35*, 1700317–n/a; c) L. Liu, H. Zhao, J. M. Andino, Y. Li, *ACS Catal.* **2012**, *2*, 1817–1828.
[9] Y. Wei, J. Jiao, Z. Zhao, J. Liu, J. Li, G. Jiang, Y. Wang, A. Duan, *Appl. Catal. B* **2015**, *179*, 422–432.

[10] a) Q. Zhang, Y. Li, E. A. Ackerman, M. Gajdardziska-Josifovska, H. Li, *Appl. Catal. A* **2011**, *400*, 195–202; b) M. Ye, X. Wang, E. Liu, J. Ye, D. Wang, *ChemSusChem* **2018**, *11*, 1606–1611.
[11] a) G. Carja, M. Birsanu, K. Okada, H. Garcia, *J. Mater. Chem. A* **2013**, *1*, 9092–9098; b) X. Meng, T. Wang, L. Liu, S. Ouyang, P. Li, H. Hu, T. Kako, H. Iwai, A. Tanaka, J. Ye, *Angew. Chem. Int. Ed.* **2014**, *53*, 11478–11482; *Angew. Chem.* **2014**, *126*, 11662–11666; c) Q. Kang, T. Wang, P. Li, L. Liu, K. Chang, M. Li, J. Ye, *Angew. Chem. Int. Ed.* **2015**, *54*, 841–845; *Angew. Chem.* **2015**, *127*, 855–859.
[12] L. Mino, G. Spoto, A. M. Ferrari, *J. Phys. Chem. C* **2014**, *118*, 25016–25026.
[13] W.-J. Yin, M. Krack, B. Wen, S.-Y. Ma, L.-M. Liu, *J. Phys. Chem. Lett.* **2015**, *6*, 2538–2545.
[14] a) B. A. Rosen, A. Salehi-Khojin, M. R. Thorson, W. Zhu, D. T. Whipple, P. J. A. Kenis, R. I. Masel, *Science* **2011**, *334*, 643; b) V. Strehmel, *ChemPhysChem* **2012**, *13*, 1649–1663.
[15] S. Wang, X. Wang, *Angew. Chem. Int. Ed.* **2016**, *55*, 2308–2320; *Angew. Chem.* **2016**, *128*, 2352–2364.
[16] A. G. Wallace, M. D. Symes, *Trends Chem.* **2019**, *1*, 247–258.
[17] a) M. Wagstaffe, M. J. Jackman, K. L. Syres, A. Generalov, A. G. Thomas, *ChemPhysChem* **2016**, *17*, 3430–3434; b) S. Malali, M. Foroutan, *J. Phys. Chem. C* **2017**, *121*, 11226–11233.
[18] H. Weber, B. Kirchner, *ChemSusChem* **2016**, *9*, 2505–2514.
[19] N. M. Simon, M. Zanatta, F. P. dos Santos, M. C. Corvo, E. J. Cabrita, J. Dupont, *ChemSusChem* **2017**, *10*, 4927–4933.
[20] A. B. Bocarsly, Q. D. Gibson, A. J. Morris, R. P. L'Esperance, Z. M. Detweiler, P. S. Lakkaraju, E. L. Zeitler, T. W. Shaw, *ACS Catal.* **2012**, *2*, 1684–1692.
[21] M. I. Qadir, M. Zanatta, E. S. Gil, H. K. Stassen, P. Gonçalves, B. A. D. Neto, P. E. N. de Souza, J. Dupont, *ChemSusChem* **2019**, *12*, 1011–1016.
[22] D. M. Tobaldi, R. C. Pullar, M. P. Seabra, J. A. Labrincha, *Mater. Lett.* **2014**, *122*, 345–347.
[23] H. Weber, T. Bredow, B. Kirchner, *J. Phys. Chem. C* **2015**, *119*, 15137–15149.
[24] J. Tao, T. Luttrell, M. Batzill, *Nat. Chem.* **2011**, *3*, 296.
[25] A. G. Thomas, W. R. Flavell, A. K. Mallick, A. R. Kumarasinghe, D. Tsoutsou, N. Khan, C. Chatwin, S. Rayner, G. C. Smith, R. L. Stockbauer, S. Warren, T. K. Johal, S. Patel, D. Holland, A. Taleb, F. Wiame, *Phys. Rev. B* **2007**, *75*, 035105.
[26] P. Chaudhari, V. Chaudhari, S. Mishra, *Mater. Res.* **2016**, *19*, 446–450.
[27] a) J. Li, H. Zhou, H. Zhuo, Z. Wei, G. Zhuang, X. Zhong, S. Deng, X. Li, J. Wang, *J. Mater. Chem. A* **2018**, *6*, 2264–2272; b) D.-N. Pei, L. Gong, A.-Y. Zhang, X. Zhang, J.-J. Chen, Y. Mu, H.-Q. Yu, *Nat. Commun.* **2015**, *6*, 8696; c) G. Wang, H. Wang, Y. Ling, Y. Tang, X. Yang, R. C. Fitzmorris, C. Wang, J. Z. Zhang, Y. Li, *Nano Lett.* **2011**, *11*, 3026–3033.
[28] a) C. Ge, K.-J. Jin, L. Gu, L.-C. Peng, Y.-S. Hu, H.-Z. Guo, H.-F. Shi, J.-K. Li, J.-O. Wang, X.-X. Guo, C. Wang, M. He, H.-B. Lu, G.-Z. Yang, *Adv. Mater. Interfaces* **2015**, *2*, 1500407; b) J. Jeong, N. Aetukuri, T. Graf, T. D. Schladt, M. G. Samant, S. S. P. Parkin, *Science* **2013**, *339*, 1402; c) K. Fujiwara, T. Ichimura, H. Tanaka, *Adv. Mater. Interfaces* **2014**, *1*, 1300108.
[29] Q. Kang, J. Cao, Y. Zhang, L. Liu, H. Xu, J. Ye, *J. Mater. Chem. A* **2013**, *1*, 5766–5774.
[30] J. Sikora, E. Sikora, D. D. Macdonald, *Electrochim. Acta* **2000**, *45*, 1875–1883.
[31] a) S. P. Harrington, T. M. Devine, *J. Electrochem. Soc.* **2008**, *155*, C381–C386; b) R. De Gryse, W. P. Gomes, F. Cardon, J. Vennik, *J. Electrochem. Soc.* **1975**, *122*, 711–712; c) S. Khan, M. J. L. Santos, C. F. Malfatti, J. Dupont, S. R. Teixeira, *Chem. Eur. J.* **2016**, *22*, 18501–18511.
[32] A. Sarkar, G. G. Khan, *Nanoscale* **2019**, *11*, 3414–3444.
[33] a) M. Zanatta, A.-L. Girard, G. Marin, G. Ebeling, F. P. dos Santos, C. Valsecchi, H. Stassen, P. R. Livotto, W. Lewis, J. Dupont, *Phys. Chem. Chem. Phys.* **2016**, *18*, 18297–18304.
[34] T. Inoue, A. Fujishima, S. Konishi, K. Honda, *Nature* **1979**, *277*, 637–638.
[35] C. C. Cassol, G. Ebeling, B. Ferrera, J. Dupont, *Adv. Synth. Catal.* **2006**, *348*, 243–248.

Manuscript received: July 15, 2020
Revised manuscript received: August 13, 2020
Accepted manuscript online: August 17, 2020
Version of record online: ■■, ■■■

# FULL PAPERS

**Hybrid theory**: An effective method to prepare $TiO_2$@IL semiconductor-liquid junctions for $CO_2$ photo-conversion is developed. The ionic liquid (IL) plays a dual role by inducing a shift of the valence band with simultaneously decreasing the band gap as well as continuous generation of formate radicals, which suggests a decrease of $CO_2$ activation energy barrier and thus improves the catalyst performance (yield and selectivity to CO).

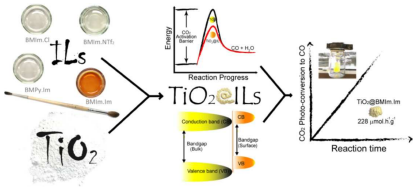


*Dr. M. I. Qadir, Dr. M. Zanatta, J. Pinto, Dr. I. Vicente, Dr. A. Gual, Dr. E. F. Smith, Prof. B. A. D. Neto, Prof. P. E. N. de Souza, Dr. S. Khan, Prof. J. Dupont*, Dr. J. Alves Fernandes**